**OAK RIDGE
NATIONAL LABORATORY**

MANAGED BY UT-BATTELLE
FOR THE DEPARTMENT OF ENERGY

Progress Report on Reversal Bending Fatigue Testing of Zry-4 Surrogate Rod
(Out-of-Cell Fatigue Testing Development, Task 2.4)

August 2013

Prepared by

**Jy-An John Wang and Hong Wang
Materials Science and Technology Division**

**Project Managers
Bruce Bevard and Rob Howard
Reactor & Nuclear Systems Division**

Oak Ridge National Laboratory

UT–BATTELLE

ORNL-27 (4-00)

Materials Science and Technology Division

PROGRESS REPORT ON
REVERSAL BENDING FATIGUE TESTING OF ZRY-4 SURROGATE ROD
(OUT-OF-CELL FATIGUE TESTING DEVELOPMENT, TASK 2.4)

Jy-An John Wang and Hong Wang
Materials Science and Technology Division

Project Managers
Bruce Bevard and Rob Howard
Reactor and Nuclear Systems Division

Date Published: August 2013

CONTENTS

LIST OF FIGURES

Figure   **Page**

LIST OF TABLES

ACKNOWLEDGMENTS

EXECUTIVE SUMMARY

Testing high-burnup spent nuclear fuel (SNF) presents many challenges in areas such as specimen preparation, specimen installation, mechanical loading, load control, measurements, data acquisition, and specimen disposal because these tasks are complicated by the radioactivity of the test specimens. Unique features of the test and testing specimens demand that the test plan address these issues from the very beginning. The main considerations for testing the high-burnup SNF rods include the following:

- High-burnup SNF rods have a composite structure with multiscale discontinuities.

- Pellet–pellet interfaces and normal stresses parallel to the longitudinal axis of the SNF rod will dominate the rod failure mechanism under cyclic bend loading during transportation.

- Shearing-dominant fractures and contact-induced damage in a conventional four- or three-point bending setup readily induce failures away from the target locations.

- A free-fixed (FRFXD) type of boundary condition is required at the specimen grip ends to ensure the rod specimen can move freely in the axial direction under bend loading, which significantly increases the degree of difficulty in U-bent apparatus design.

- Installation of the testing setup in a hot-cell environment imposes strict constraints on the test design.

An extensive literature survey revealed a variety of developed bending fatigue testing methods, including cantilever beam bending, three- or four-point bending, and pure bending, as well as environmental-factor considerations, particularly temperature. However, these conventional systems cannot meet the challenges and constraints uniquely related to the vibration integrity study of SNF rod.

The research and comparison studies conducted at Oak Ridge National Laboratory (ORNL) resulted in a new concept for the U-frame testing setup to perform hot-cell reversal bending fatigue testing in 2010. Subsequently the three-dimensional finite element analysis and engineering design of components were completed. The first prototype of the U-frame was assembled and mounted to an MTSservo-hydraulic testing machine in June 2011. Many issues with the reversal cyclic bending were raised during the calibration and testing even though proof-of-concept had been demonstrated. The technical challenges included a proper specimen hold, effective implementation of the FRFXD boundary condition, and mitigation of the components' weight on sample bending deformation. From 2012 to 2013 the ORNL team finalized the upgrade of the U-frame testing setup and the integration of the U-frame setup into a Bose dual linear motor test bench. A final check was conducted on the test system in August 2013, and the system is ready to be delivered to the hot cell.

The fatigue responses of Zircaloy-4 (Zry-4) cladding and the role of pellet-pellet and pellet-clad interactions are critical to the SNF vibration integrity, but such data are not available due to the unavailability of an effective testing system, as mentioned above. While the deployment of the developed test system in a hot cell will provide the opportunity to generate the data, the use of a surrogate rod has proven quite effective in identifying the underlying deformation mechanism of an SNF composite rod under an equivalent loading condition.

This report presents the experimental results of using surrogate rods under reversal cyclic loading. Specifically, monotonic and cyclic bending tests were conducted on surrogate rods made of a Zry-4 tube and alumina pellets, both with and without an epoxy bond. The conclusions drawn based on the test results and initial data analysis are described below.

- The surrogate rod with an epoxy bond appeared to be much stronger than the rod without an epoxy bond for both monotonic and cyclic loading cases. The epoxy-bond rod exhibited a brittle failure, while no appreciable failure could be seen for the rod without the epoxy bond, even though the curvature of the rod reached the equivalent deformation level.

- The surrogate rods with an epoxy bond fractured under cyclic bending for load amplitude greater than 100N, with lifetime of between 104 and 106 loading cycles. No failure was seen at the 100 N load level at loading cycles up to 2 million cycles. An S-N curve is clearly defined for the cyclic test of epoxy-bond rods.

- The use of 10 Hz frequency in the cyclic test apparently accelerated the fatigue aging, which shortened the lifetime of the surrogate rod under a defined load level. A more detailed analysis regarding the potential dynamic inertia effect on the experimental results is needed, as is could provide further benchmarks and clarification of the fatigue data obtained at higher-frequency bend loading conditions.

- No defined S-N trend was obtained for the rods without an epoxy bond, which could be the result of the uncertainties in the specimen machining condition, gap configuration at pellet–pellet and pellet–clad interfaces, and the use of various testing conditions.

1. INTRODUCTION

Testing high-burnup spent nuclear fuel (SNF) presents many challenges in areas such as specimen preparation, specimen installation, mechanical loading, load control, measurements, data acquisition, and specimen disposal because these tasks are complicated by the radioactivity of the test specimens. Unique features of the test and testing specimens demand that the test plan address these issues from the very beginning. The main considerations for testing the high-burnup SNF rods include the following:

- High-burnup SNF rods have a composite structure with multiscale discontinuities.

- Pellet–pellet interfaces and normal stresses parallel to the longitudinal axis of the SNF rod will dominate the rod failure mechanism under cyclic bend loading during transportation.

- Shearing-dominant fractures and contact-induced damage in a conventional four- or three-point bending setup readily induce failures away from the target locations.

- A free-fixed (FRFXD) type of boundary condition is required at the specimen grip ends to ensure the rod specimen can move freely in the axial direction under bend loading, which significantly increases the degree of difficulty in U-bent apparatus design.

- Installation of the testing setup in a hot-cell environment imposes strict constraints on the test design.

An extensive literature survey revealed a variety of developed bending fatigue testing methods, including cantilever beam bending, three- or four-point bending, and pure bending, as well as environmental-factor considerations, particularly temperature. However, these conventional systems cannot meet the challenges and constraints uniquely related to the vibration integrity study of SNF rod.

The research and comparison studies conducted at Oak Ridge National Laboratory (ORNL) resulted in a new concept for the U-frame testing setup to perform hot-cell reversal bending fatigue testing in 2010.[1] Subsequently the three-dimensional finite element analysis and engineering design of components were completed. The first prototype of the U-frame was assembled and mounted to an MTSservo-hydraulic testing machine in June 2011.[2] Many issues with the reversal cyclic bending were raised during the calibration and testing even though proof-of-concept had been demonstrated. These issues covered a variety of areas from including installation of the rod specimen, measurement of rod bending, to the selection of the driving system for the hot cell, etc. The technical challenges included a proper specimen hold, effective implementation of the FRFXD boundary condition, and mitigation of the components' weight on sample bending deformation.[3]

From 2012 to 2013 the ORNL team finalized the upgrade of the U-frame testing setup and the integration of the U-frame setup into a Bose dual linear motor test bench.[4] A final check was conducted on the test system in August 2013, and the system is ready to be delivered to the hot cell.

The fatigue responses of Zircaloy-4 (Zry-4) cladding and the role of pellet-pellet and pellet-clad interactions are critical to the SNF vibration integrity, but such data are not available due to the unavailability of an effective testing system, as mentioned above. While the deployment of the developed test system in a hot cell will provide the opportunity to generate the data, the use of a surrogate rod has proven quite effective in identifying the underlying deformation mechanism of an SNF composite rod under an equivalent loading condition.

This report presents the experimental results of using the surrogate rods made of Zry-4 cladding and alumina pellets under reversal cyclic bend loading

2. REVERSAL BENDING FATIGUE TEST SYSTEM

The reversal bending fatigue test system is composed of a U-frame testing setup for imposing bending loads on the spent fuel rod test specimen and a method for measuring the curvature of the rod during bending.[5] The U-frame setup consists of two rigid arms, linking members, and linkages to a universal testing machine. A horizontal layout of the U-frame setup is adopted to eliminate the effect of the components' weight on the bending of the rod specimen. The effect of weights has been found to be substantial enough that the bending of the rod can deviate from the pure bending condition. Dual linear motors (Bose ElectroForce System Dual LM2 TB, MN) are used to apply the point forces symmetrically at the two loading points. These linear motors use the electromagnetic force in driving and have been shown to be more advantageous in hot-cell testing than other conventional actuation systems such as servo-hydraulic and electromechanical. In addition, it has been demonstrated that the use of the two linear motors can benefit the symmetrical loading as well, especially in the dynamic loading such as that to be tested in hot cell. As a result, the reciprocal motion of tow loading rod points is converted into reversal bending of the rod specimen that is integrated into the U-frame.

The current U-frame setup can accommodate a 152.40 mm (6 in.) rod specimen whose diameter can be from 9.50 to 11.70 mm. The rod is coupled to the U-frame using two rigid sleeves that have an inside diameter (ID) of 15.00 mm, outside diameter (OD) of 25.00 mm, and length of 50.80 mm. The sleeves themselves are mounted to the specimen ends using cast epoxy. A vise mold is made to be used for this purpose; therefore, a gauge section of 50.80 mm (2 in.) is obtained once the specimen is installed to the U-frame.

The dual linear motors are mounted to a breadboard along with the U-frame setup. The system can deliver a load capacity of +/-3000 N and displacement of +/-25.40 mm. The current setup is equipped with a 101.60 mm (4 in.) loading arm, so the maximum available moment of system for bending is +/-304.80 Nm. The interface components assembled on Bose dual LM2 TB are shown in Fig. 1.

(a)

(b)

Fig. 1. (a) U-frame setup integrated to Bose dual LM2 TB, (b) the enlarged view of specimen section with three LVDTs mounted to simultaneously measure the deflections of the rod at three points.

3. PREPARATION OF ROD SPECIMEN

Two 5 ft Zry-4 tubes with OD 9.50 mm and ID 8.36 mm were received and sectioned into twenty 6 in. short tubes. At the same time, ten 5/16 in. × 12 in. alumina rods were purchased from McMaster-Carr. Each rod was then cut into 15.24 mm small rods. These small rods serve as pellets within the 6 in. Zry-4 cladding tube.

The pellet–cladding interaction was studied through simulations with and without epoxy bonding. Preparation of epoxy-bond surrogate rods involved installing the alumina pellet along with the injecting epoxy on the internal surface of the cladding tubes and end faces of the pellets. The cladding tubes loaded with alumina pellets were then used in the next stage in which the rigid sleeves were mounted.

The mounting of two rigid sleeves onto the rod specimen was accomplished using a vise mold. For the first rigid sleeve, mounting required injecting the epoxy into the sleeve, transferring the sleeve to the chamber of the vise mold, inserting the rod, and closing the mold. For the second sleeve, only epoxy injection and transfer of the rigid sleeve was necessary. A 24 h curing period was generally needed to allow the epoxy to reach full strength, and then the rod specimen was detached using the handle. The detailed procedure is provided in Wang et al. 2013.[4]

A commercial epoxy (3M DP420, MN) dual pack was used in this research. The studies demonstrated that the cast epoxy can serve as a compliant layer with the required durability in both cycle fatigue and hot-cell radiation environments. [5,4]

The specimens were designated as ZRAPxx for the surrogate rods made of Zry-4 cladding (with "xx" indicating the sample number) and alumina pellets with epoxy bonding and as ZRAPMxx for those without the bonding.

4. TEST PROCEDURE

4.1 MONOTONIC TEST

Monotonic testing was conducted under displacement control. The displacement channels of the test machine were set at a load rate of 0.2 mm/s to 10.00 mm and back to 0 mm at the same rate. Such displacement control is equivalent to a unidirectional 0.01Hz triangle wave. Because the dual linear motors and U-frame setup are connected in series, the applied displacement to the U-frame is accumulated. Thus, the total (or relative) maximum displacement in the test was 20.00 mm.

As mentioned above, the bend of the rod was measured by using three linear variable differential transformers (LVDTs). Although the deflections themselves provided information related to rod's deformation, it has been shown that these measurements involve additional contribution from the compliant layer; therefore, the curvature was used in this study to characterize the bending of the rod. The test results are presented in Sect. 5 of this report in terms of moment–curvature curves.

4.2 CYCLE TEST

The reversal cyclic bending testing consisted of (1) measurements at the specified number of cycles and (2) the cycling itself. The measurements included three cycles of 0.05 Hz sine waves with peak displacements of ±0.4, ±0.6, and ±0.8 mm.

The cycling involved using 5 or 10 Hz sine waves under load control. The determination of the load amplitudes depended on the experimental results from monotonic test. In general, the selected load amplitude captured lifetimes at 10^4, 10^5, and 10^6 cycles.

The cycle test stopped whenever the following events occurred: (1) the predetermined limits in displacement 1 or 2 exceeded 4 to 6 mm or (2) the accumulative cycle number exceeded 1 or 2 million.

Data of displacements, loads, and LVDTs were acquired during both the measurements and cycling at defined sampling rate and intervals. The moment-curvature curvatures were carefully examined and validated for each test. The curvature range, moment range, and flexural rigidity (moment per unit curvature)[5] were used in this study and are provided in Sect. 6 of this report.

5. RESULTS OF MONOTONIC TEST

The resistance of the U-frame to loading can be substantial, especially when the monotonic test demands a large displacement, with average readings of load channels as high as 40 N near the 10.00 mm displacement channels. With this regard, the load channel readings were corrected to take into account the resistant force from the system.

5.1   SURROGATE ROD WITH EPOXY BOND

Results for ZRAP01 and ZRAP02 are shown in Figs. 2 and 3. The loading results initially show a linear response, followed by a nonlinear stage with three unloading valleys before the peak point. These unloading valleys correspond to popping sounds emitted during the test. Optical microscopy of ZRAP01 revealed that multiple transverse cracks had developed (Fig. 4); therefore, the unloading points observed on the loading curve for ZRAP01 may be related to the cracking events. In the case of ZRAP02, however, no crack can be seen on the surface of rod, so it remains unclear whether the multiple unloading valleys correspond to cracks inside or outside the cladding tube.

The detailed examination of the moment–curvature plot for each test showed a transition stage existing between 10 and 20 Nm. The loading before 10 Nm and after 20 Nm corresponded to two linear stages. A rigidity of 27.8 to 32 Nm was obtained through linear regression analysis of the initial stage. This value is quite close to the theoretical prediction assuming 10% of the full alumina rod rigidity is used.

(a)

(b)

(c)
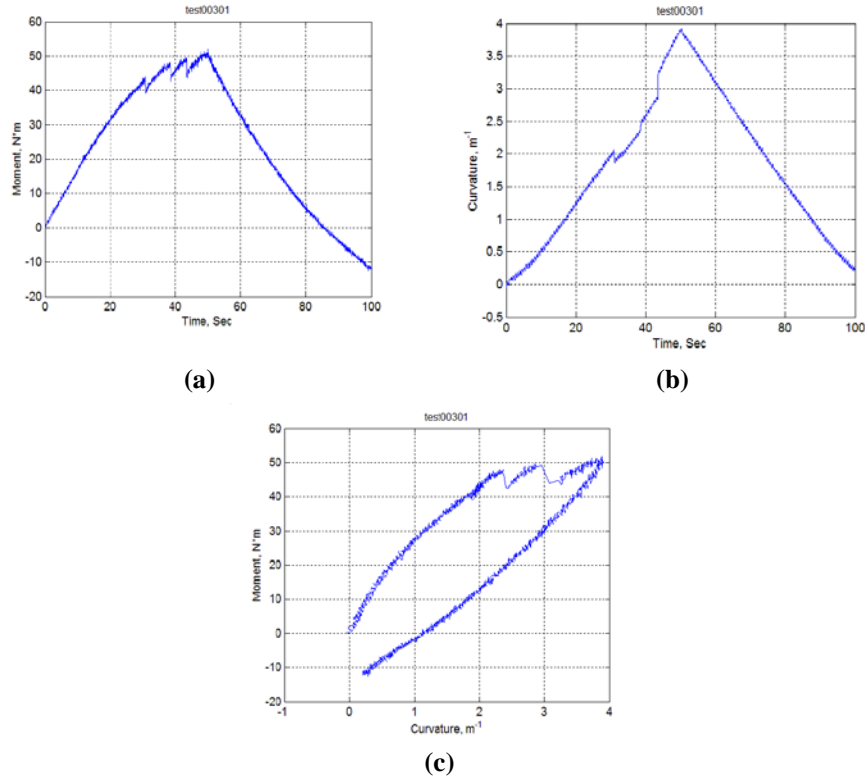
Fig. 2. (a) Moment, (b) curvature, and (c) moment–curvature curve for static bending test of ZRAP01 under 0.2 mm/s and maximum relative displacement of

20 mm at loading points of U-frame setup.

(a)

(b)

(c)
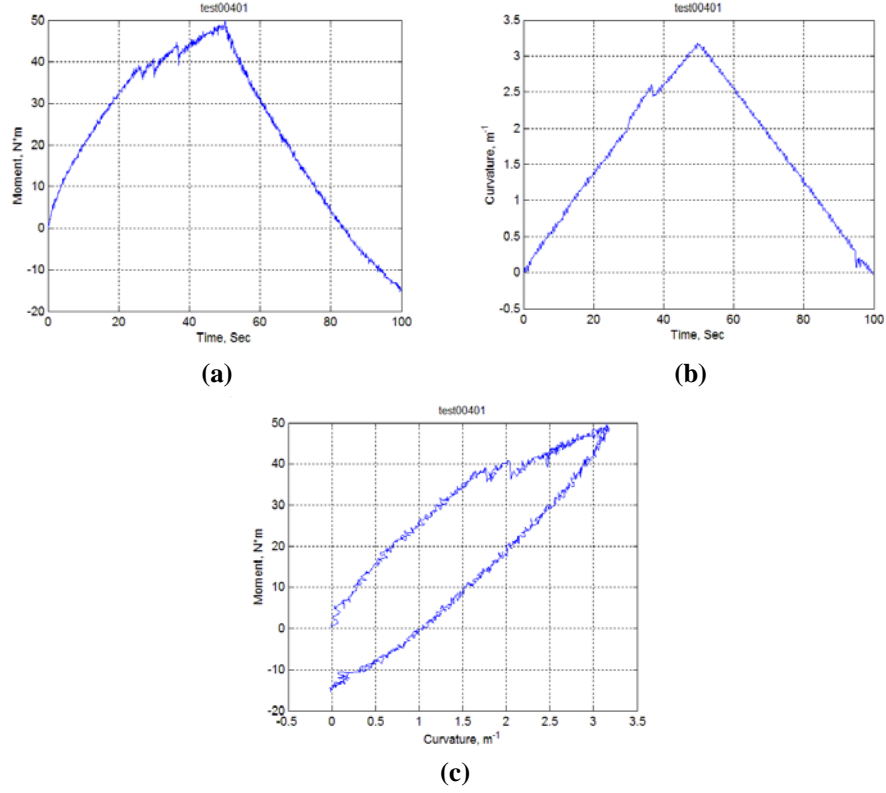
Fig. 3. (a) Moment, (b) curvature, and (c) moment–curvature curve for static bending test of ZRAP12 under 0.2 mm/s and maximum relative displacement of 20 mm at loading points of U-frame setup.
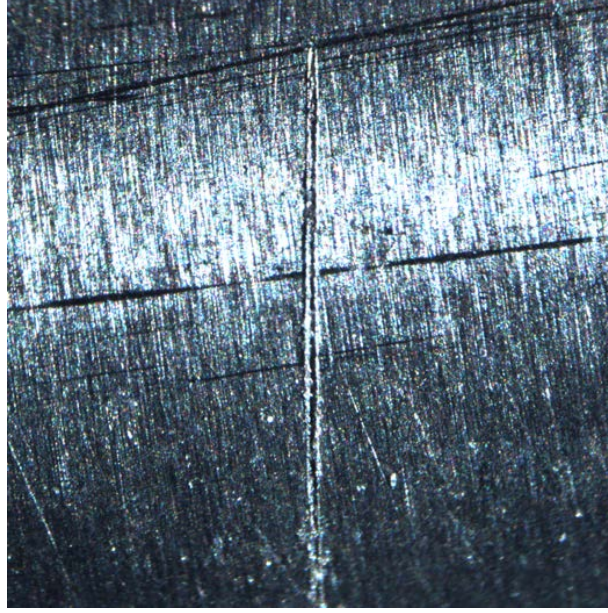
**Fig. 4. Multiple transverse cracks developed on
the surface of ZRAP01 during monotonic loading.**

Although the microprocess that dictated the behavior of the rod in this stage is unclear, it is believed that the yielding of cladding and debonding of epoxy played critical roles in accelerating the fatigue of the rod to be examined. Therefore, the range of 10 to 20 Nm, or 100 to 200 N at the loading points of the U-frame, was set as the target amplitude range for the cyclic test discussed below. Later the upper bound of the load range was extended to 300 N to expand the range of the lifetime of the rod at the left end.

5.2   SURROGATE ROD WITHOUT EPOXY BOND

The results for the rod specimen without an epoxy bond, ZRAPM01, are given in Fig. 5. It is interesting to see that both the maximum curvature and moment obtained under the same relative displacement of 20.00 mm are lower than those of ZRAP01. In particular, the maximum moment decreased from 50 Nm to 35 Nm. The estimate of flexural rigidity based on the initial linear stage of moment curvature resulted in a value of 14.5 Nm. This level of rigidity matches the theoretical prediction only if the contribution of alumina pellets is omitted; therefore, the impact of the epoxy bond on the response of the rod under bending is substantial.

At the same time, the range of load amplitudes used in the cycle tests described in Sect. 6 was the same as that for rods with an epoxy bond.
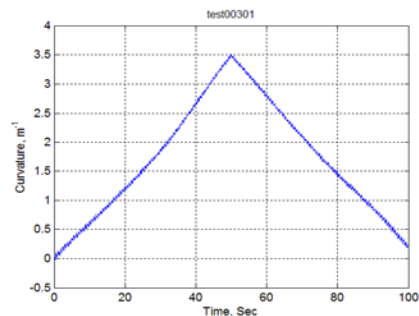
(a)   (b)
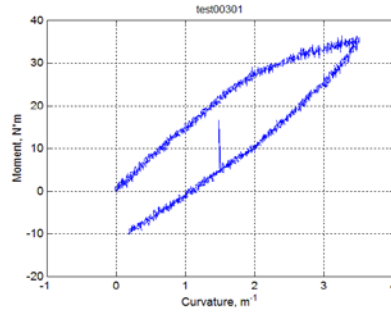
(c)

Fig. 5. (a) Moment, (b) curvature, and (c) moment–curvature curve for static bending test of ZRAPM01 under 0.2 mm/s and maximum displacement of 20 mm at loading points of U-frame setup.
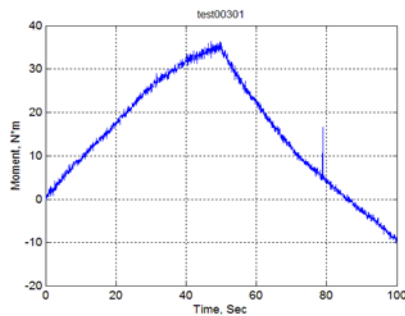
11

6. RESULTS OF CYCLE TEST

6.1 SUMMARY

A summary of the results for the cycle tests conducted in this project along with monotonic tests and calibration is provided in Table 1. The relationship of the moment to the number of cycles is given in Fig. 6.

For the epoxy-bond case, the rod fractures were observed for most of the cyclic tests with moments more than 10 Nm. On the other hand, the fractures were observed for the no-epoxy-bond case in all of the moment levels.

The following sections discuss the fatigue test results for the surrogate rods, particularly in terms of flexural rigidity. This quantity can be monitored online, making it quite promising for characterizing the fatigue response of reversal bending rods.

Table 1. Summary of Zry-4 Surrogate Rod Tests

| Specimen No.	Epoxy	Mode	Control	Amp.* (mm, N)	Amp. (mm, N*m)	Freq. (Hz)	Lifetime (N or Nf)	Notes
ZRAP01	Bond	Monotonic	Displacement	20	20	0.01		
ZRAP02	Bond	Cycle	Load	100	10.16	5	1.27E+06	No failure
ZRAP03	Bond	Cycle	Load	200	20.32	5	4.06E+04	Fractured
ZRAP04	Bond	Cycle	Load	150	15.24	5	5.49E+05	Fractured
ZRAP05	Bond	Calibration	Load	80	8.128	1,5,10		
ZRAP06	Bond	Cycle	Load	200	20.32	10	7.25E+03	Fractured
ZRAP07	Bond	Cycle	Load	200	20.32	10	6.38E+03	Fractured
ZRAP08	Bond	Cycle	Load	100	10.16	10	2.00E+06	No failure
ZRAP09**	Bond	Cycle	Load	150	15.24	5	2.22E+06	Fractured
ZRAP10	Bond	Cycle	Load	175	17.78	5	5.86E+04	Fractured
ZRAP11	Bond	Cycle	Load	200	20.32	5	4.17E+04	Fractured
ZRAP12	Bond	Cycle	Displacement	10	10	0.01		
ZRAP13	Bond	Cycle	Load	250	25.4	5	1.10E+04	Fractured
ZRAP14	Bond	Cycle	Load	300	30.48	5	3.32E+03	Fractured
ZRAPM01	None	Monotonic	Displacement	20	20	0.01		
ZRAPM02	None	Cycle	Load	200	20.32	5	6.71E+03	Fractured
ZRAPM03	None	Cycle	Disp	150	15.24	5	2.31E+04	Fractured
ZRAPM04	None	Cycle	Disp	100	10.16	10	7.44E+03	Fractured

* For the displacement, the amplitude means that a relative displacement at the two load points of the U-frame was used.
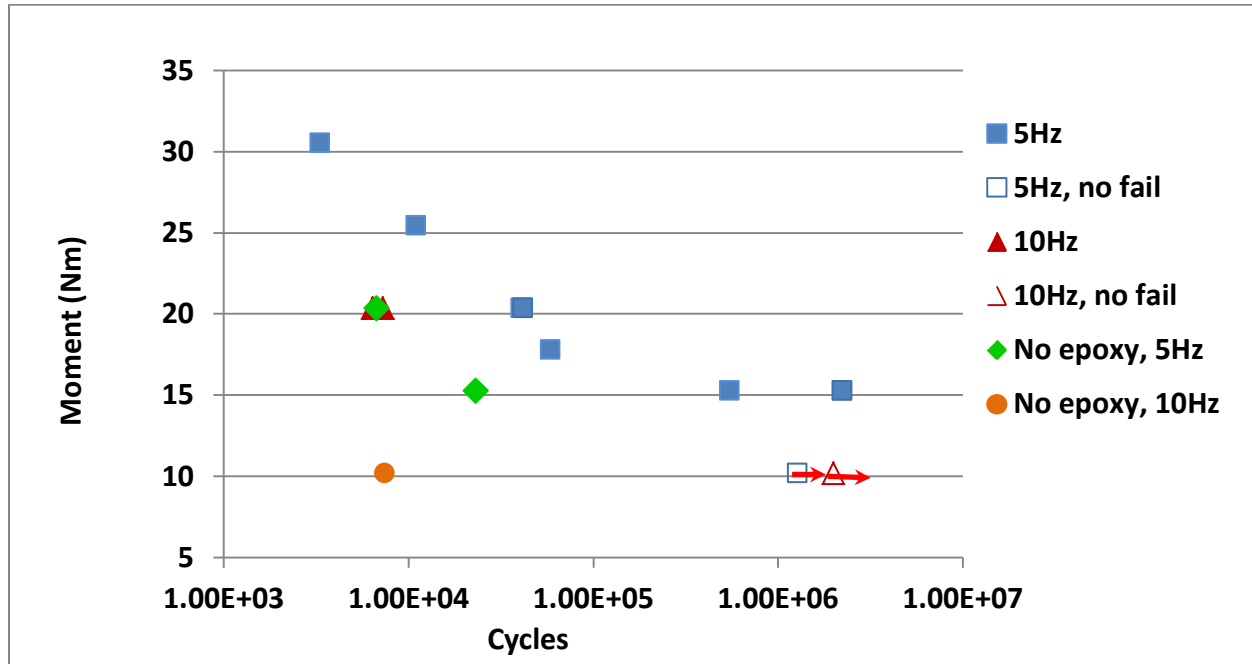** The last 79,000 cycles used 10 Hz in the cycle test.

Fig. 6. Summary of cycle tests of Zry-4 surrogate rods.

6.2 SURROGATE ROD WITH EPOXY BOND

The resistance of the system under dynamic loading or a cycle test was found to be at the noise level, and therefore, the data processing of dynamic testing will not involve the data correction required for static loading mainly because the level of loading amplitude is generally relatively small compared to that used in static loading.

6.2.1 5 Hz Cycle Tests

The results of the 5 Hz cycle tests are presented in Figs. 7 to 14 for ZRAP02–ZRAP04, ZRAP09-11, ZRAP13, and ZRAP14, respectively. Except for that of ZRAP02, all of the rigidity fatigue curves demonstrated a continuous decrease over the entire course of the cyclic test. The continuous degradation was also observed for ZRAP09, whose test (+/-150 N, 5 Hz) went beyond 2 million cycles. The specimen fractured shortly after the test was switched to 10 Hz to accelerate the fatigue. Another important observation is that for those fractured or cracked specimens, the degradation rate did not seem to change very much during the cyclic test, even when the specimen was about to fracture.

The results based on measurements exhibited variation comparable to those from online monitoring data. The selected curvature ranges for measurements allowed the bend of the rod to fall within the elastic region of the moment–curvature curve. These curvature ranges for measurements were all equal to or less than those used in cycling; therefore, the effect of measurement on the cycling is not believed to have been substantial, as validated by the concurrent changes of rigidity in both processes. For example, in the case of ZRAP02, the rigidity curves based on measurements were quite settled within a defined region, while that of online rigidity was correspondingly stabilized near the 35 Nm level.

Figure 15 exhibits the fractured rods of specimens ZRAP03, ZRAP04, ZRAP09, ZRAP10, and ZRAP11. It can clearly be seen that all of failures occurred in the gauge section, as designed. The micrograph in

Fig. 16 shows a part of rod ZRAP13 in which the fracture also occurred in the gauge section. The two transverse cracks (about 2 to 3 mm long) can clearly be seen to have coalesced near a surface flaw.

(a)

(b)

(c)

(d)

(e)

Fig. 7. Variation of (a) curvature, (b) moment, and (c) rigidity based on online monitoring; measurement results for (d) curves of moment versus curvature and (e) flexural rigidity versus curvature of ZRAP02: ±100 N, 5 Hz; no failure observed.

14

Fig. 8. Variation of (a) curvature, (b) moment, and (c) rigidity based on online monitoring; measurement results for (d) curves of moment versus curvature and (e) flexural rigidity versus curvature of ZRAP03: ±200 N, 5 Hz.

(a)

(b)

(c)

(d)

(e)

Fig. 9. Variation of (a) curvature, (b) moment, and (c) rigidity based on online monitoring; measurement results for (d) curves of moment versus curvature and (e) flexural rigidity versus curvature of ZRAP04: ±150 N, 5 Hz.
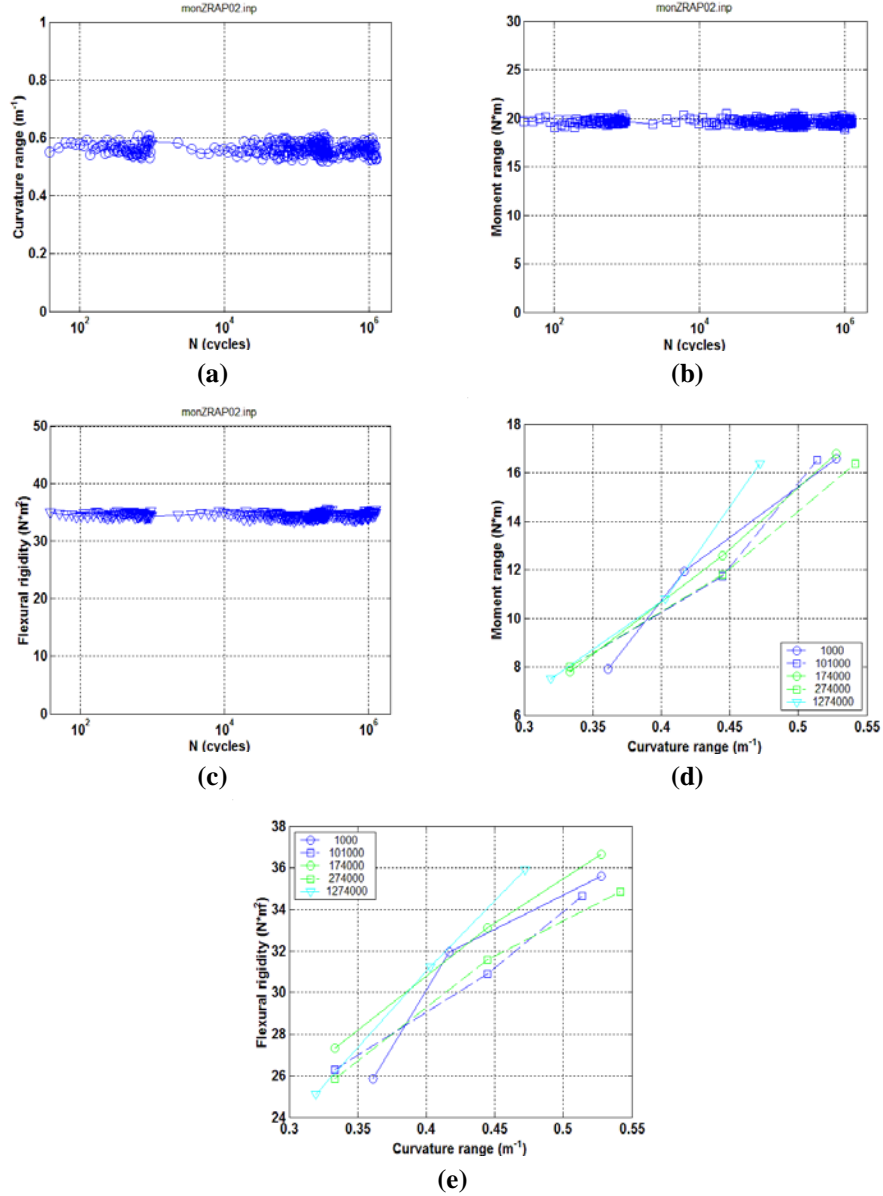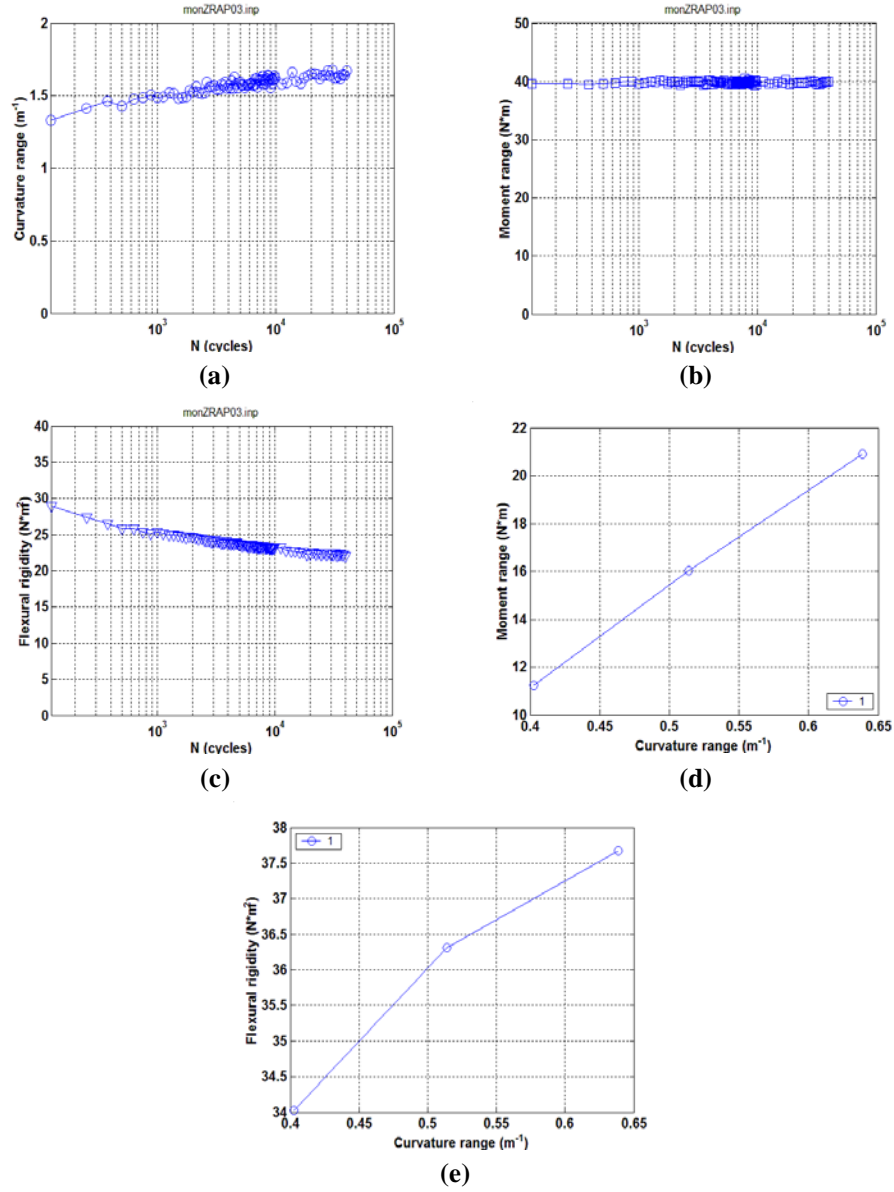
16

Fig. 10. Variation of (a) curvature, (b) moment, and (c) rigidity based on online monitoring; measurement results for (d) curves of moment versus curvature and (e) flexural rigidity versus curvature of ZRAP09: ±150 N, 5 Hz.
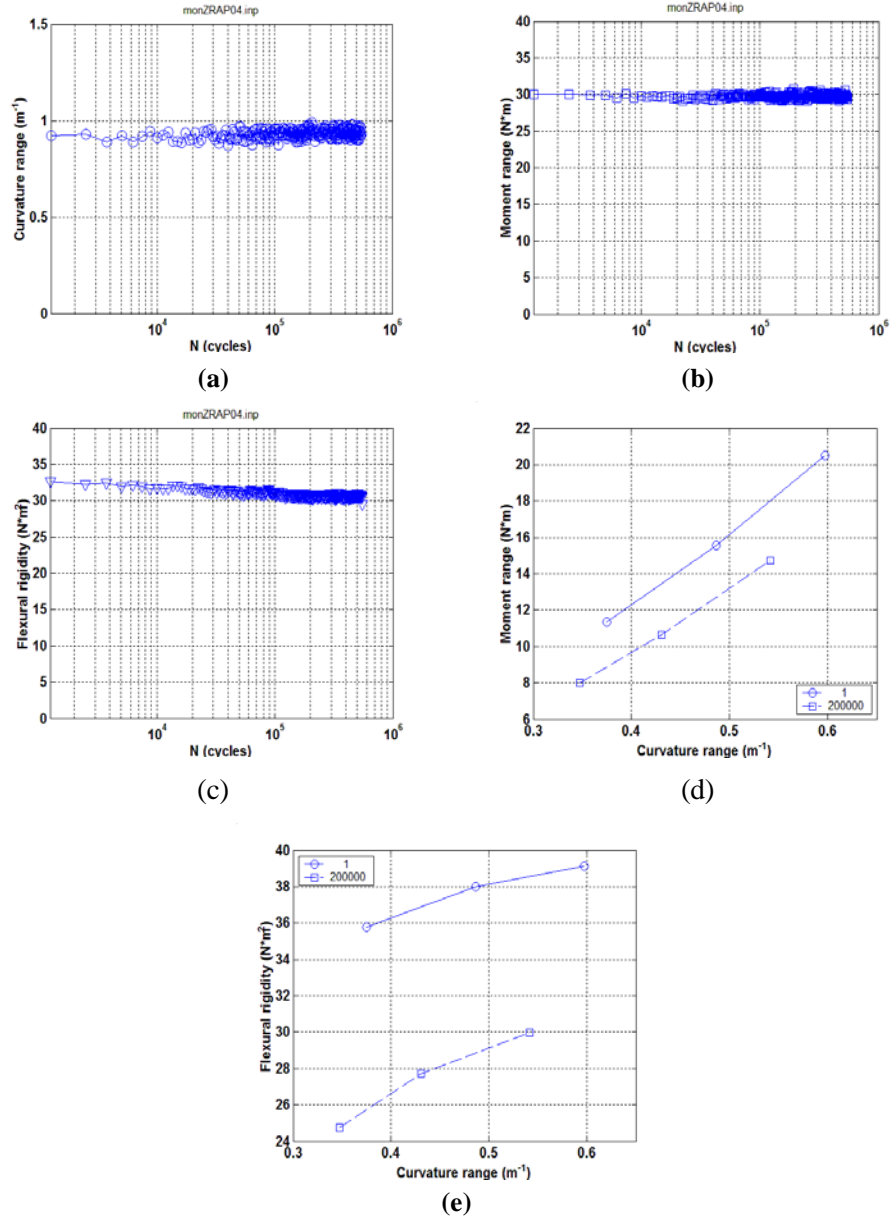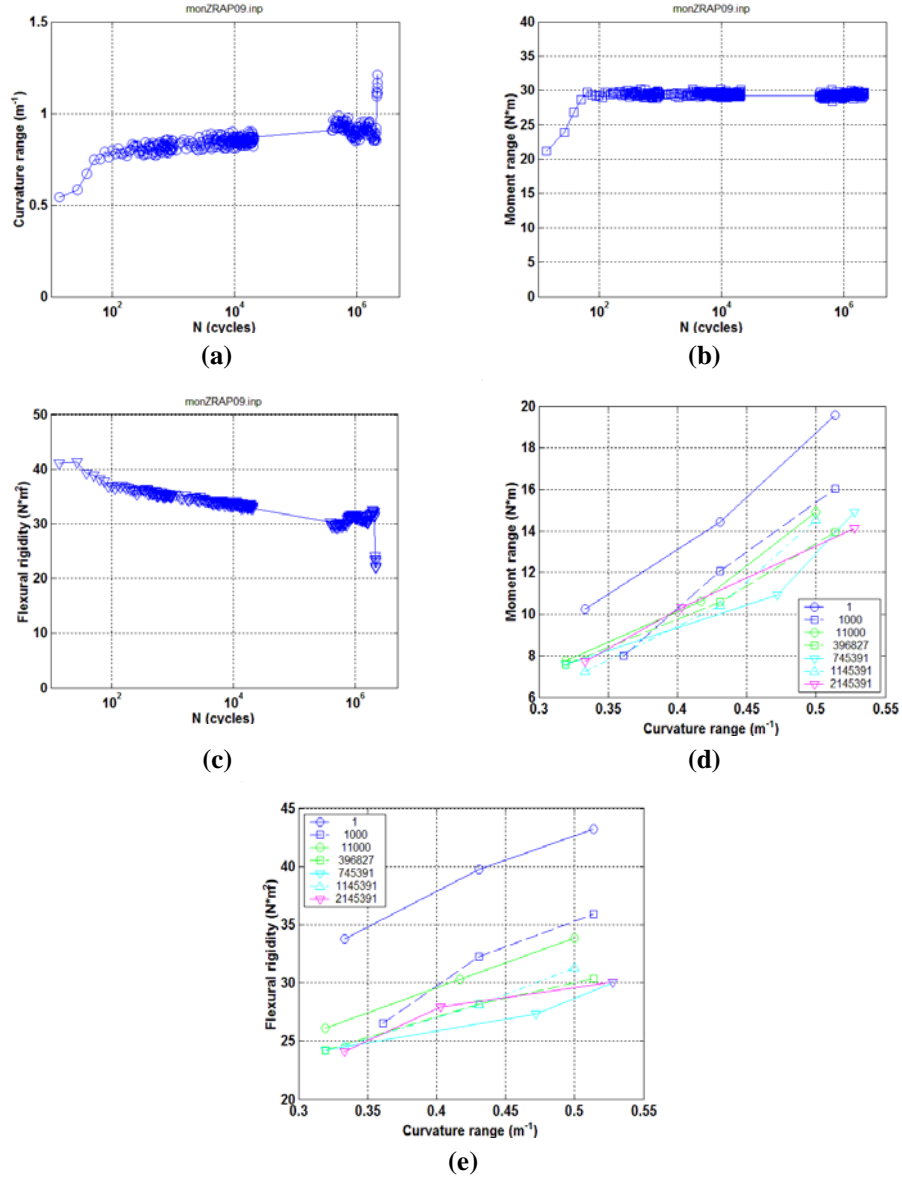
Fig. 11. Variation of (a) curvature, (b) moment, and (c) rigidity based on online monitoring; measurement results for (d) curves of moment versus curvature and (e) flexural rigidity versus curvature of ZRAP10: ±175 N, 5 Hz.

Fig. 12. Variation of (a) curvature, (b) moment, and (c) rigidity based on online monitoring; measurement results for (d) curves of moment versus curvature and (e) flexural rigidity versus curvature of ZRAP11: ±200 N, 5 Hz.

(a)

(b)

(c)

(d)

(e)

Fig. 13. Variation of (a) curvature, (b) moment, and (c) rigidity based on online monitoring; measurement results for (d) curves of moment versus curvature and (e) flexural rigidity versus curvature of ZRAP13: ±250 N, 5 Hz.
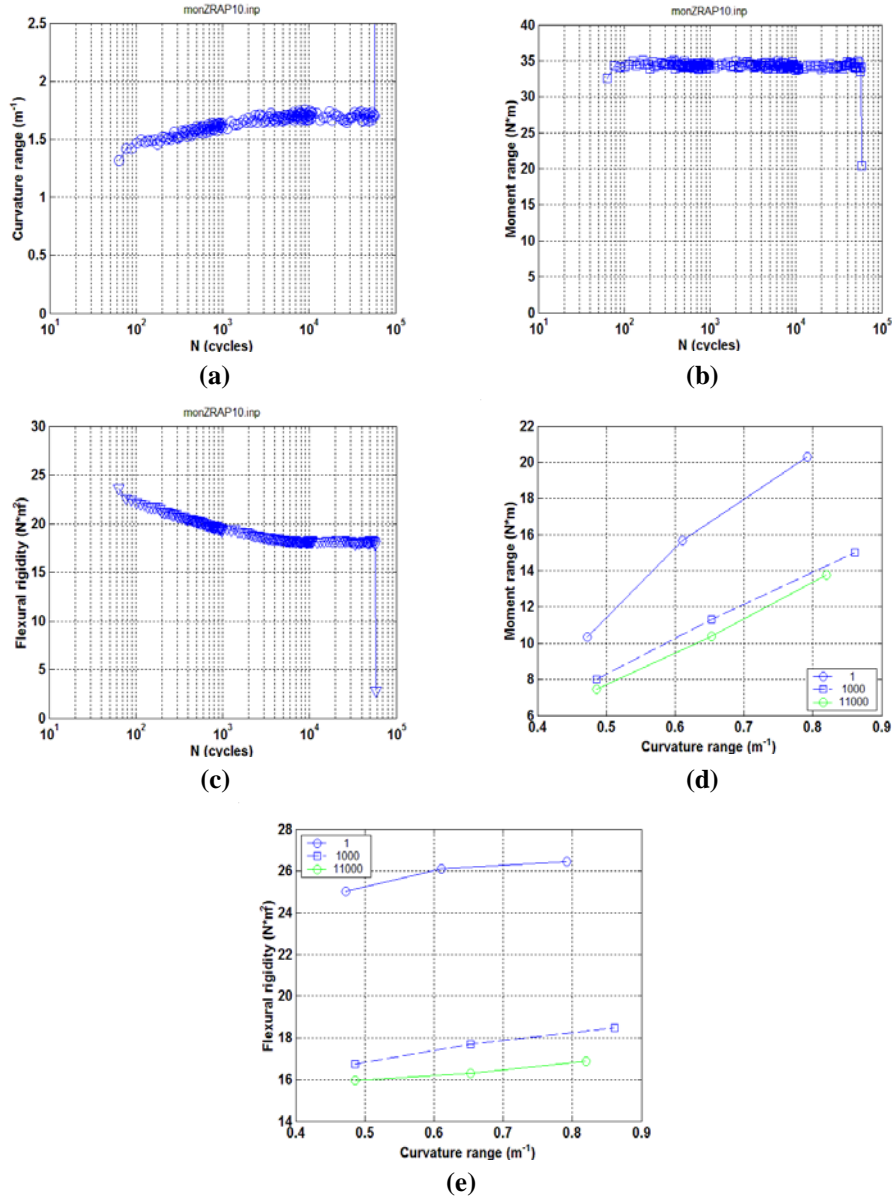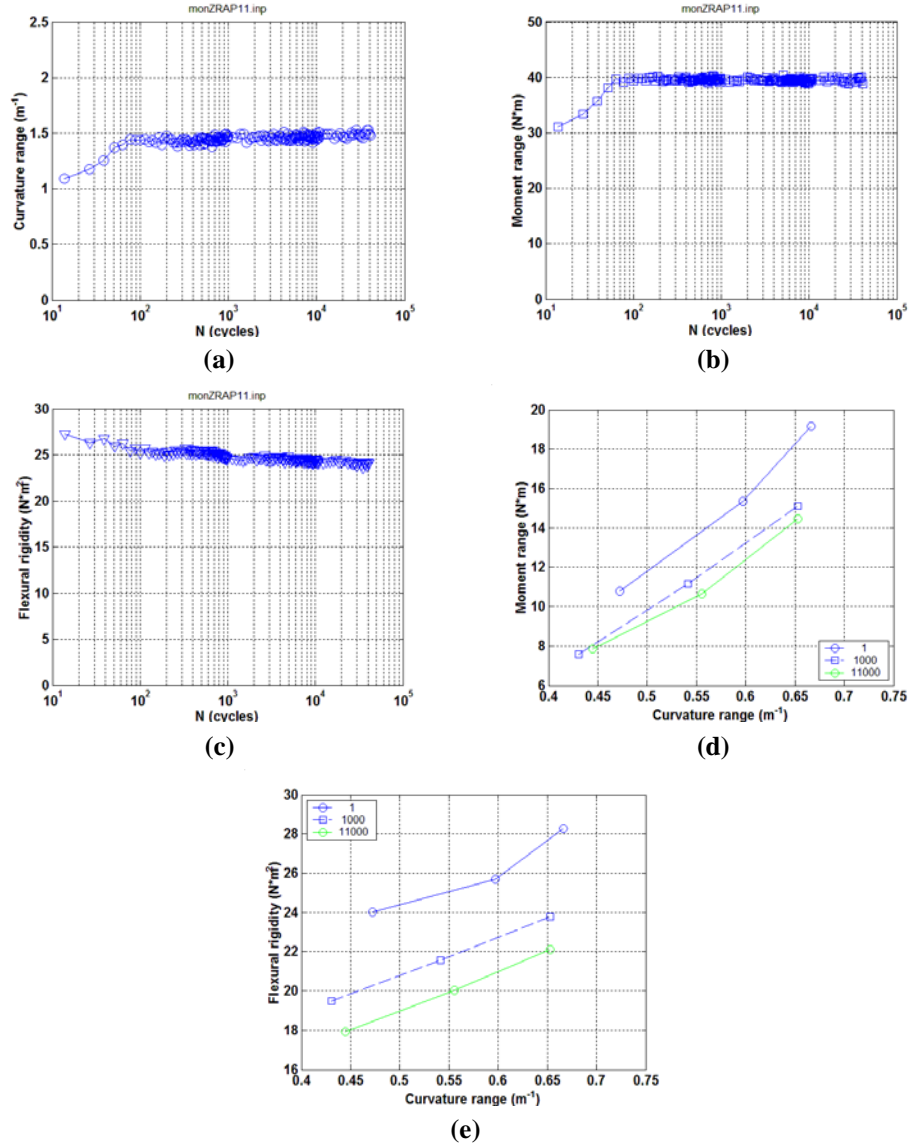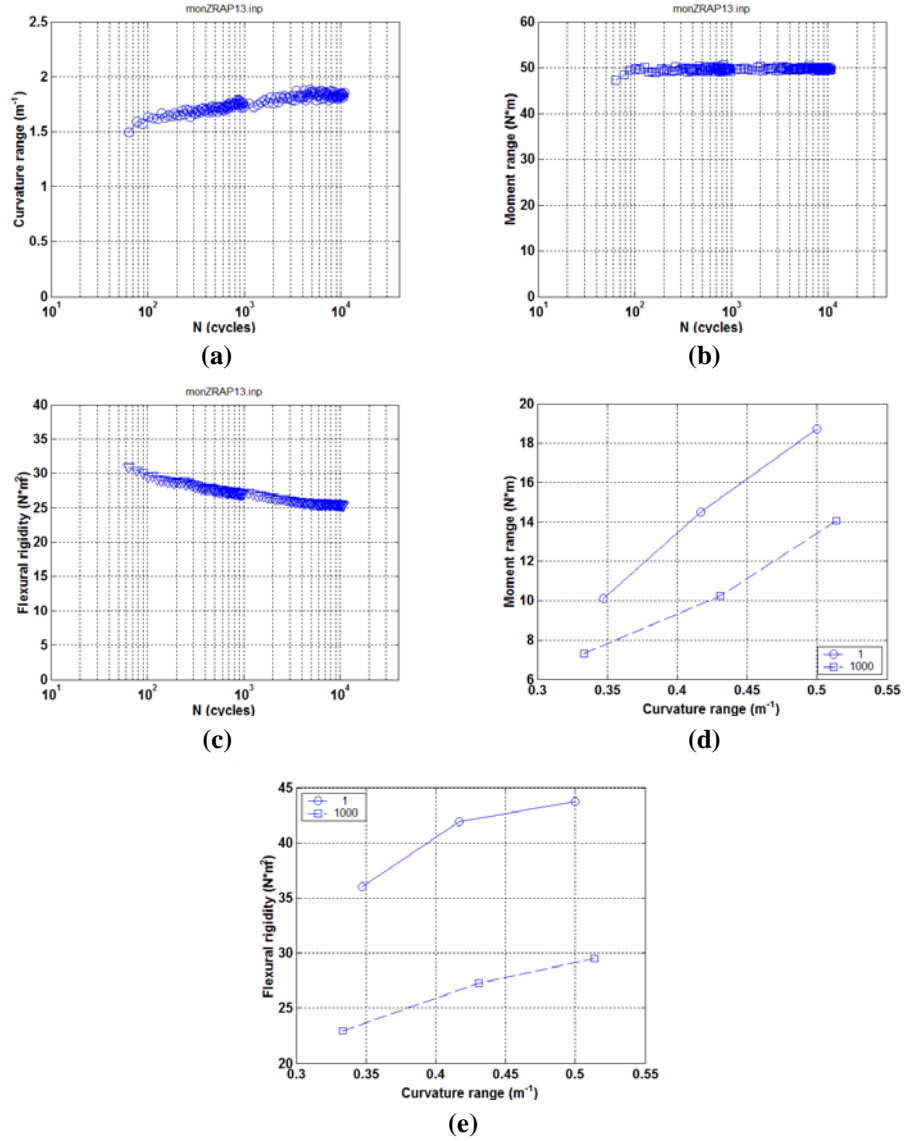
Fig. 14. Variation of (a) curvature, (b) moment, and (c) rigidity based on online monitoring; measurement results for (d) curves of moment versus curvature and (e) flexural rigidity versus curvature of ZRAP14: ±300 N, 5 Hz.

Fig. 15. Images showing fractured rods for (a) ZRAP03, (b) ZRAP04, (c) ZRAP09, (d) ZRAP10, and (e) ZRAP11.
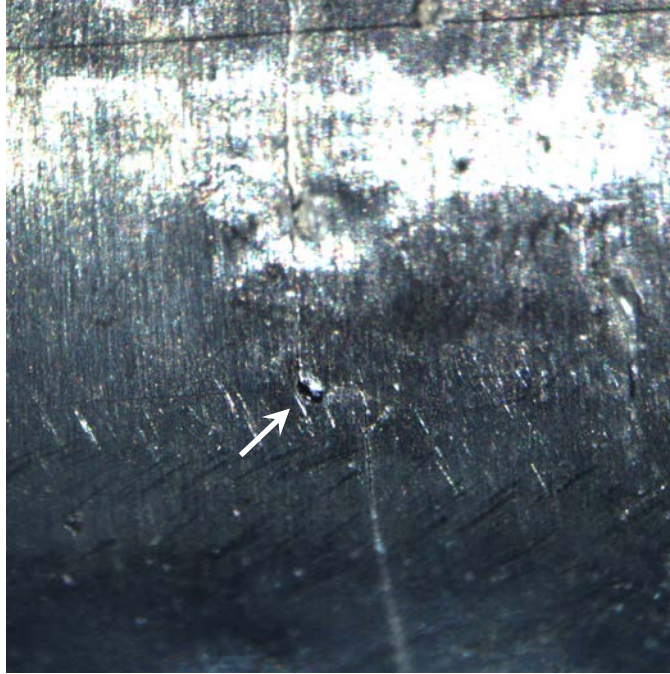
Fig. 16. Micrograph of part of the surface of ZRAP13 rod showing transverse fracture of about 4 mm length kinked near a surface flaw.

6.2.2   10 Hz Cycle Tests

The results of the 10 Hz cycle tests for epoxy-bond rods are shown in Figs. 17–19 for ZRAP06, ZRAP07, and ZRAP09, respectively. The initial starting stage of the cyclic test, in which the load changed continuously while the testing machine itself was adjusting to the target load level, is not included in these figures. Nevertheless, the system usually reached the plateau in about 100 s for the defined condition. The part of the fatigue curves presented, therefore, corresponds to the stage at which the load level was quite constant.

The failure mode of fractured rods is shown in Fig. 20, and again it can be seen that all of the failures occurred in the gauge sections.
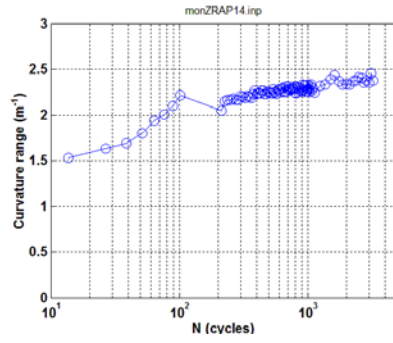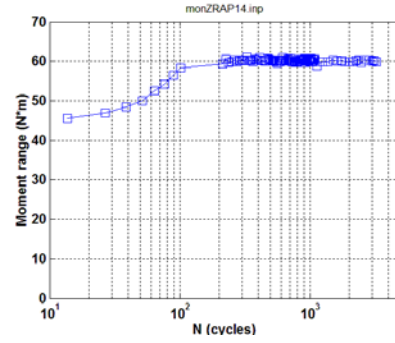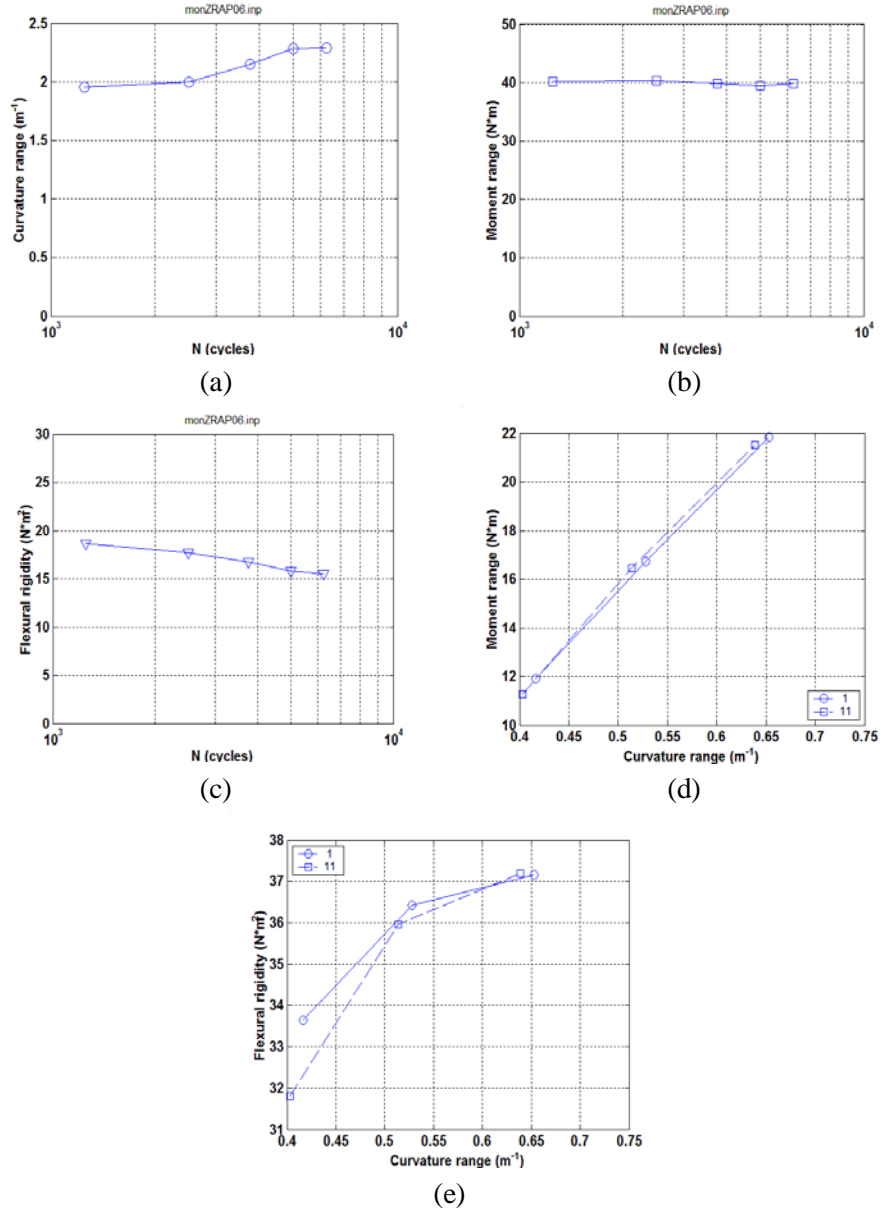
Fig. 17. Variation of (a) curvature, (b) moment, and (c) rigidity based on online monitoring; measurement results for (d) curves of moment versus curvature and (e) flexural rigidity versus curvature of ZRAP06: ±200 N, 10 Hz.
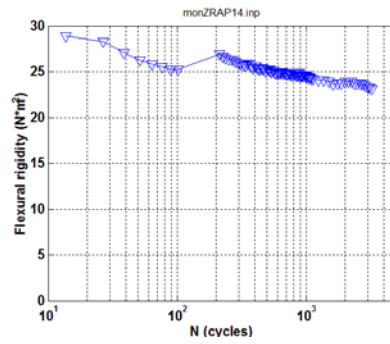
24

Fig. 18. Variation of (a) curvature, (b) moment, and (c) rigidity based on online monitoring; measurement results for (d) curves of moment versus curvature and (e) flexural rigidity versus curvature of ZRAP07: ±200 N, 10 Hz.
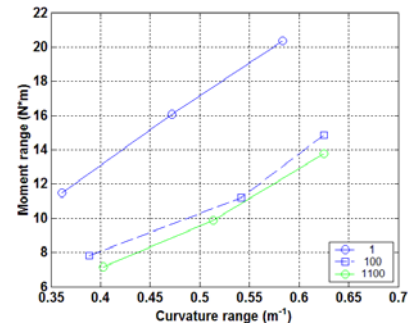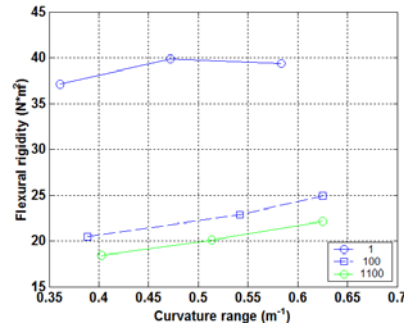
Fig. 19. Variation of **(a)** curvature, **(b)** moment, and **(c)** rigidity based on online monitoring; measurement results for **(d)** curves of moment versus curvature and **(e)** flexural rigidity versus curvature of ZRAP08: ±100 N, 10 Hz.

<div align="center">(a)   (b)</div>

Fig. 20. Images showing the fractured rods of (a) ZRAP06 and (b) ZRAP07.

6.3   SURROGATE ROD WITHOUT EPOXY BOND

Cycle tests for rods with no epoxy bond were conducted using both 5 and 10 Hz. The 5 Hz tests were used for two high amplitudes, 150 and 200 N, and the 10 Hz test was used in low amplitude, 100 N. The use of 10 Hz in the 100 N cycle test represented an attempt to accelerate the fatigue test because that amplitude was expected to generate a long lifetime.

As expected, the rods without an epoxy bond exhibited a relative short lifetime compared to those of the epoxy-bond rods. Under both 200 and 150 N, the rigidity continuously decreased prior to the fracturing of rod specimen, as shown in Figs. 21 and 22.

The test of ZRAPM04 under a low load revealed a surprisingly shorter lifetime (Fig. 23) than those under high loads. The rigidity based on online monitoring data was found to be near 7 Nm. Such low rigidity suggests that a structural flaw might be involved. Looking at the rigidity curve based on measurements, one can see that the flexural rigidity of this rod was still around 19 Nm when the curvature range was near 0.5 m^{-1}. That level of rigidity is quite comparable to those of similar rods without an epoxy bond, as shown in Figs. 21 and 22. It is believed that ramping up of the load to the designed load level (100 N) during the 10 Hz cycle test clearly triggered the structural flaw, causing a marked increase in curvature, as shown in Fig. 23(a).

The failure modes of the rods are illustrated in Fig. 24. All of the fractures are shown to have occurred within the gauge section. The examination indicated that the fractures of ZRAPM02 and ZRAPM03 seemingly originated from the surface indentations.
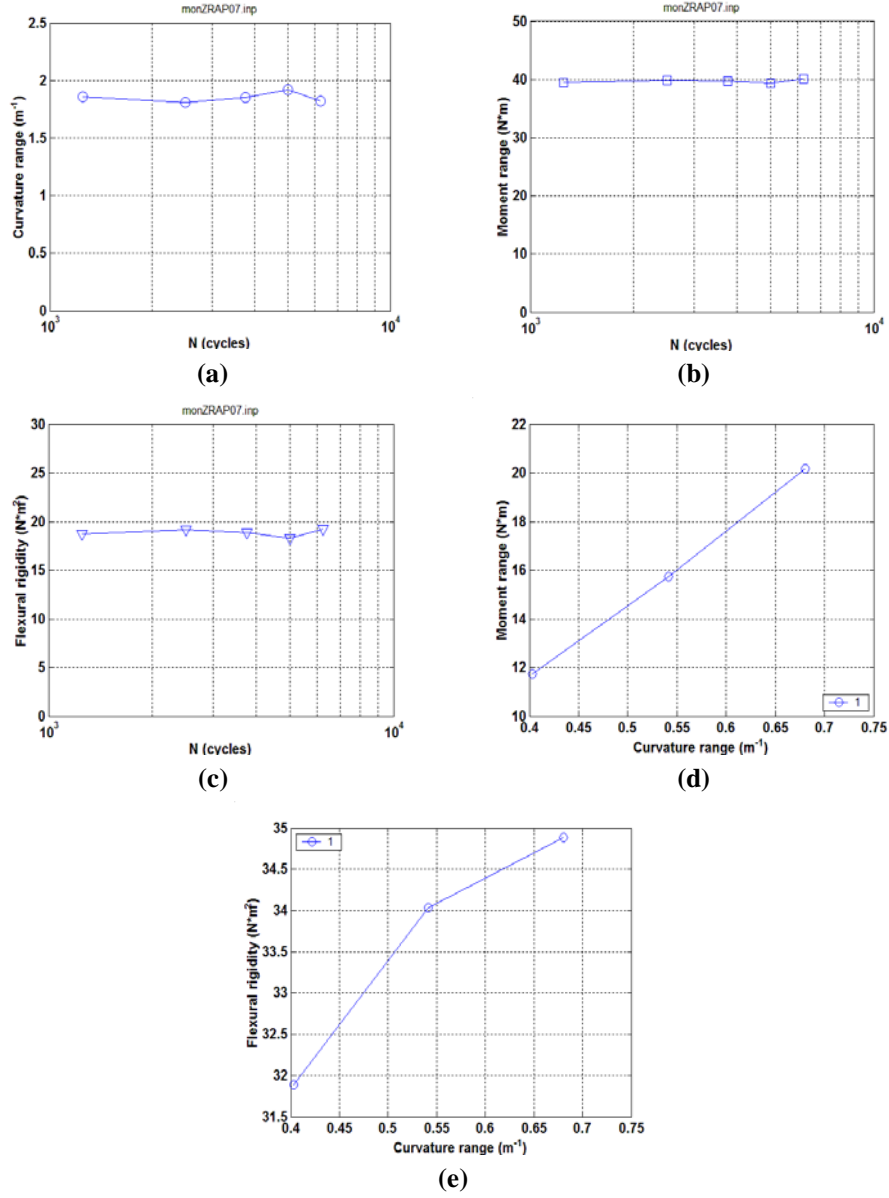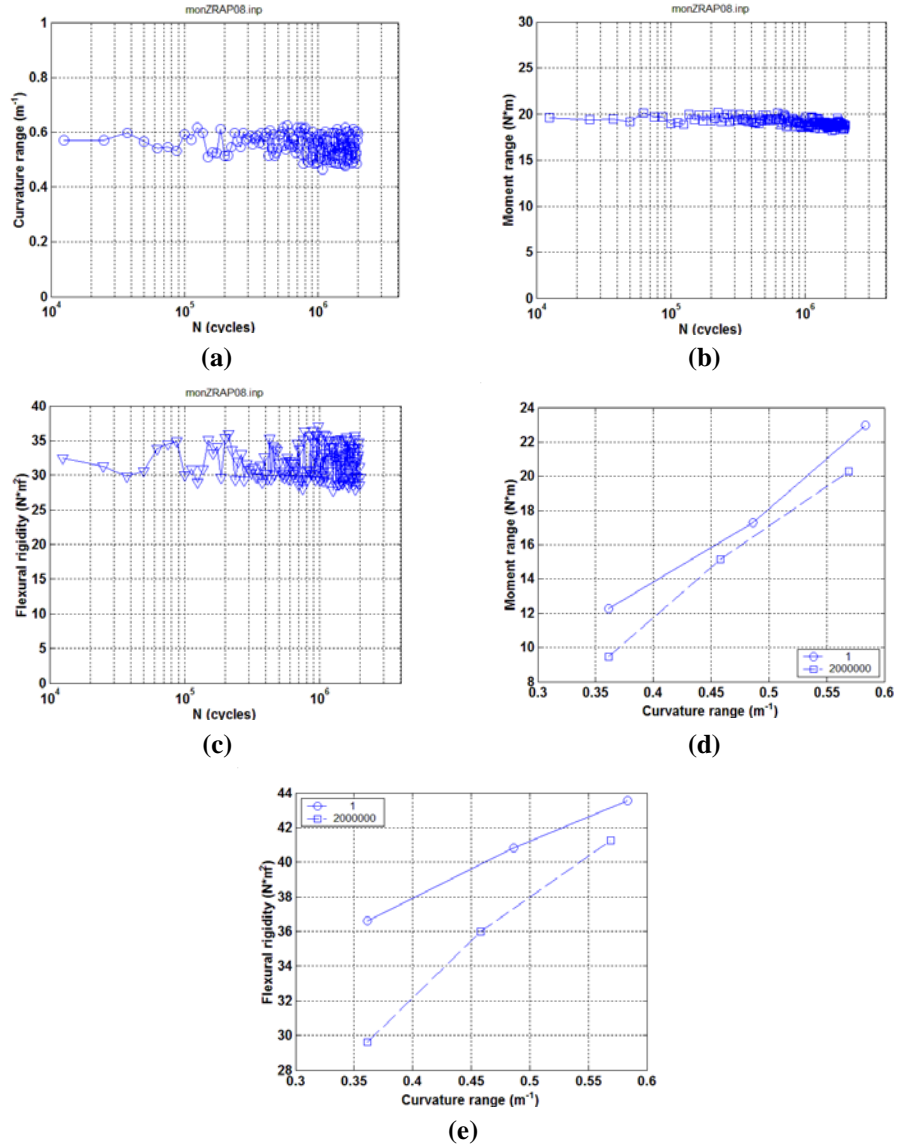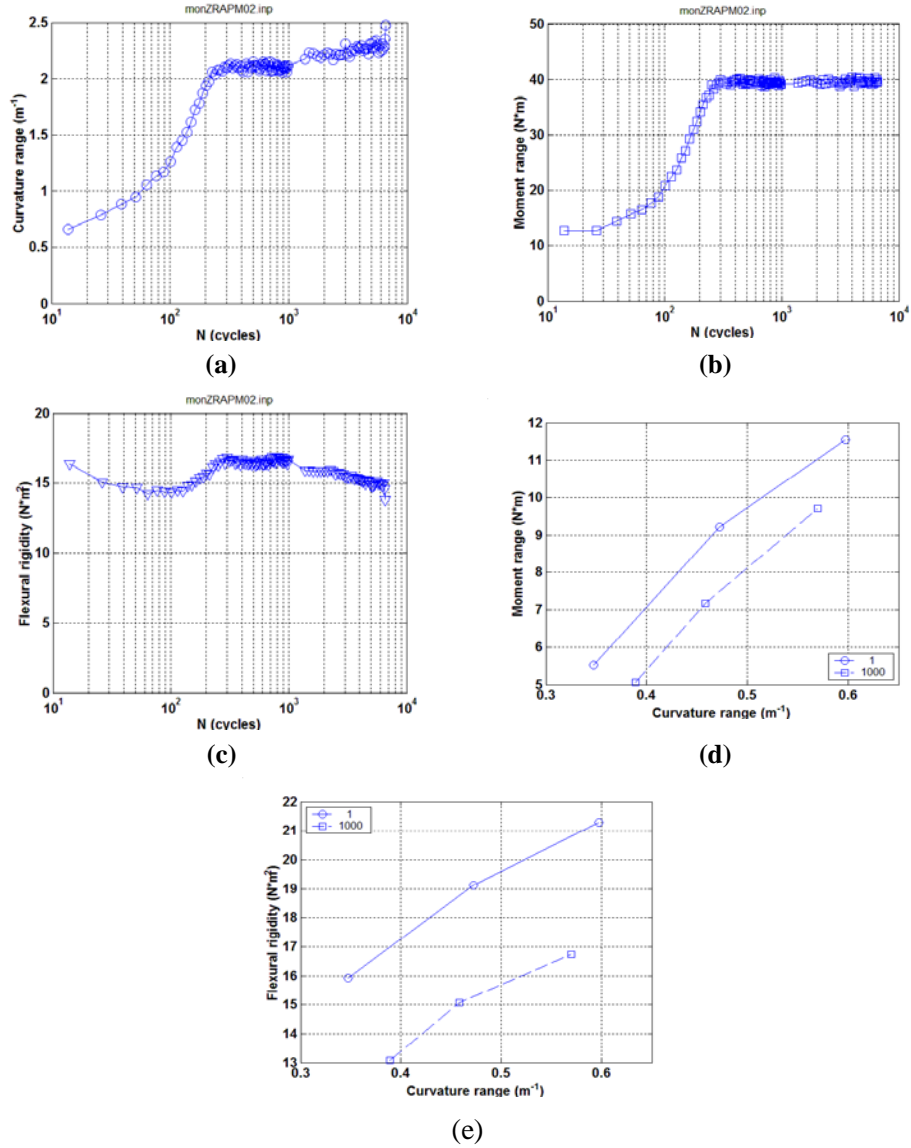
Fig. 21. Variation of (a) curvature, (b) moment, and (c) rigidity based on online monitoring; measurement results for (d) curves of moment versus curvature and (e) flexural rigidity versus curvature of ZRAPM02: ±200 N, 5 Hz.
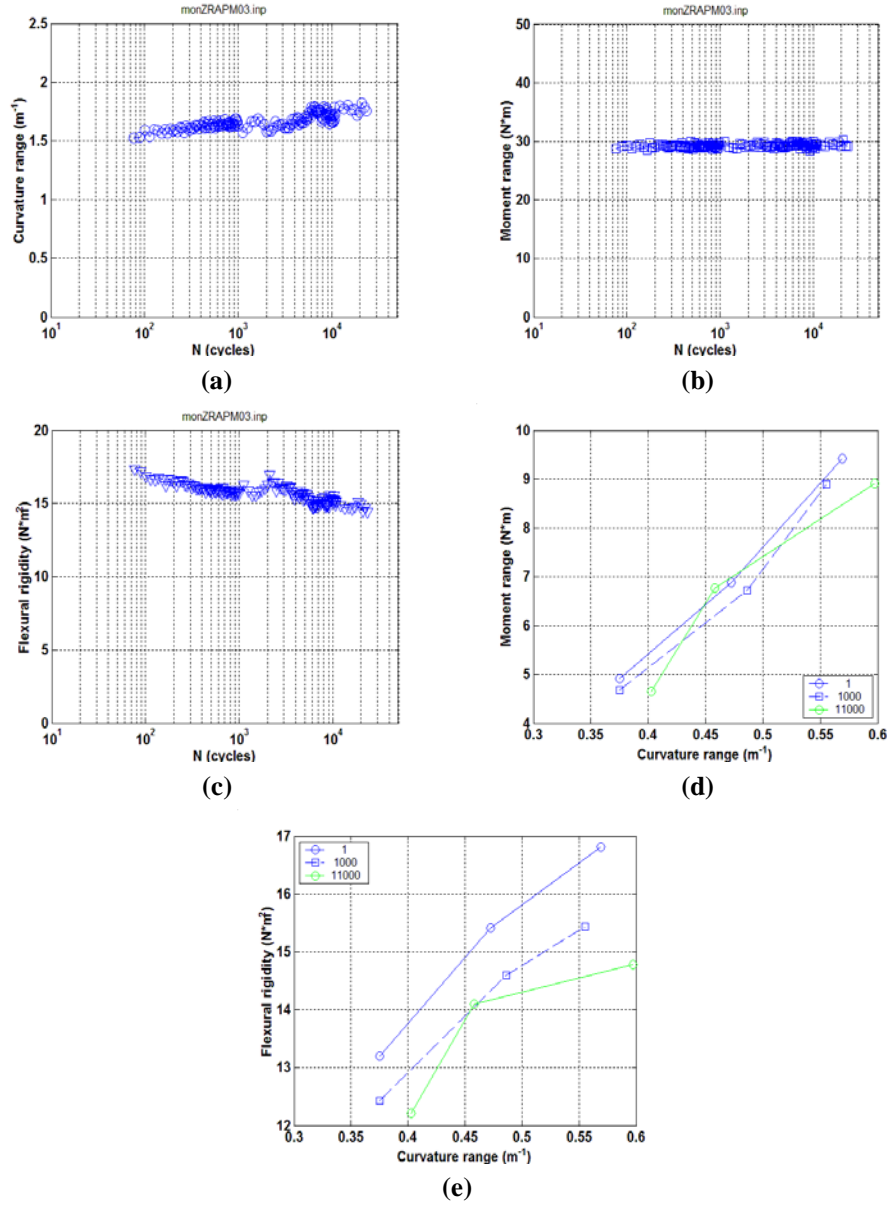
Fig. 22. Variation of (a) curvature, (b) moment, and (c) rigidity based on online monitoring; measurement results for (d) curves of moment versus curvature and (e) flexural rigidity versus curvature of ZRAPM03: ±150 N, 5 Hz.

Fig. 23. Variation of (a) curvature, (b) moment, and (c) rigidity based on online monitoring; measurement results for (d) curves of moment versus curvature and (e) flexural rigidity versus curvature of ZRAPM04: ±100 N, 10 Hz.
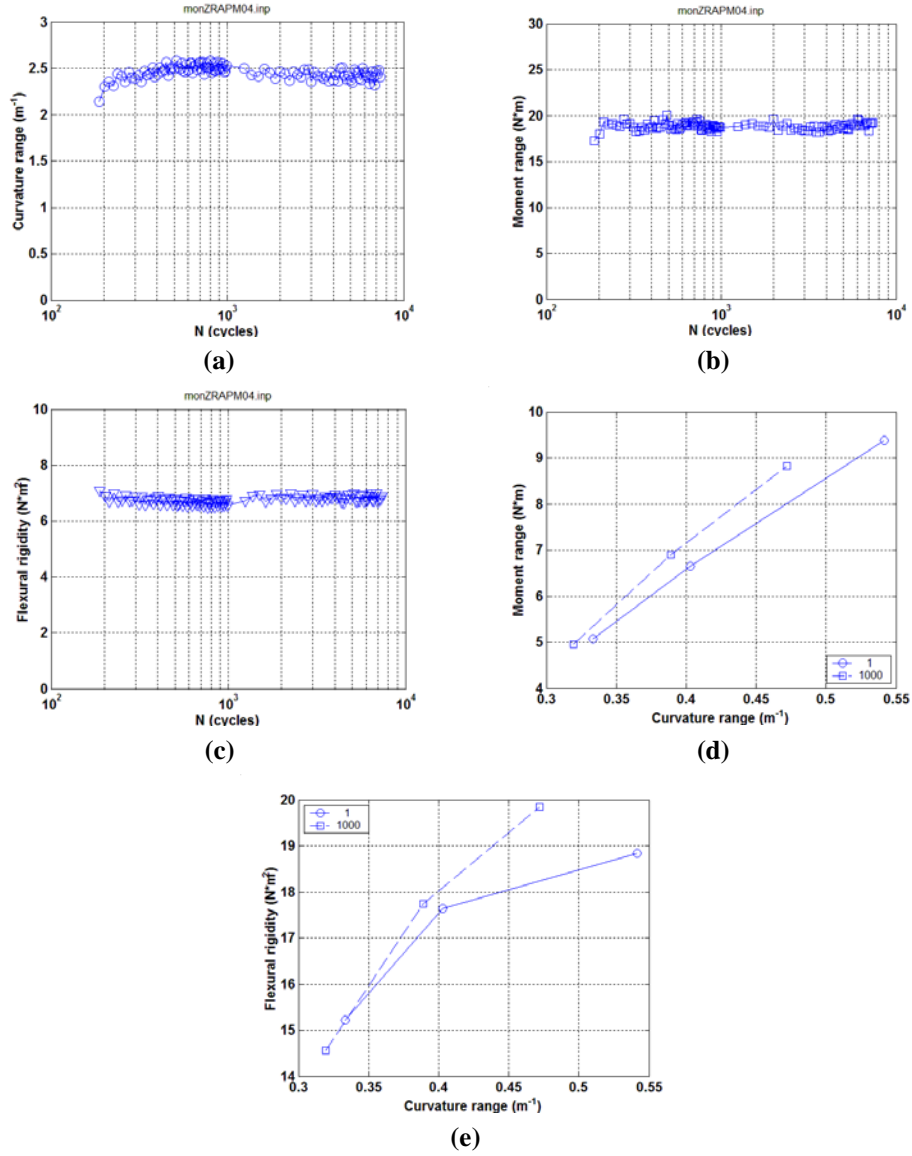
(a)

(b)

(c)

Fig. 24. Images showing fractured rods of (a) ZRAPM02, (b) ZRAPM03, and (c) ZRAPM04.

7. DISCUSSION AND CONCLUSIONS

7.1 DISCUSSION

7.1.1 Monotonic Test

The monotonic test plays an important role in evaluating the vibration response of surrogate rods. Selection of appropriate amplitudes suitable for the cyclic tests critical for the monotonic bending test result of a rod specimen. The cyclic test results showed that within the target life of 10^4 to 10^6 cycles, a couple of tests ran up to several millions cycles without rod failure. Therefore, the uncertainty related to the fabrication of a Zry-4 tube and preparation of a surrogate rod specimen could have a direct impact on the variability of test results. At least three to five specimens are needed to define the appropriate load amplitudes for cyclic tests. In a hot-cell fatigue strength evaluation, the effect of the abovementioned uncertainties on the test's outcome would be even more severe than that observed in the out-of-cell tests using surrogate rods because of inherent structural flaws and complex residual stress profiles embedded in a high burnup SNF system.

In the fatigue strength evaluations, the maximum load amplitude was selected near the beginning of the nonlinearity observed in the monotonic moment-versus-curvature curve; the onset of the nonlinear regions is a result of clad yielding and other damage mechanism associated with geometry nonlinearity and structural flaws within the composite rod. Currently the selections of target load level and load intervals for fatigue tests are largely based on the trial and error. However, the uncertainty of this process would be minimized when more controlled data are available.

7.1.2 Cycle Test

ORNL has also been working on developing a fatigue testing protocol using high frequency for the hot-cell application. This change is essential with regard to budget constraints because by making it one can significantly reduce hot-cell use, thereby lowering the overall cost of the project. However, there are certainly constraints or limits on driving the system into the higher-frequency application from both the U-frame-setup and testing-machine perspectives. The frequency response of the Bose testing machine appears to be flat from DC to 40 Hz, but the inherent dynamic property of the U-frame is the key that dictates the overall system frequency response in conjunction with the surrogate rod specimen.

Limiting the load level within the linear elastic range, the measured curvature on ZRAP05 was demonstrated to have increased by specific degrees with the increases in test frequency from 1 to 10 Hz. An understanding of the controlled dynamic mechanisms of such accelerated aging will require further system investigation on a U-bent apparatus as well as development of more valid controlled data. Nevertheless, the dynamic factor should be considered when reconciling the lifetime differences between 5 and 10 Hz cycles, as shown in Fig. 6.

7.2 CONCLUSIONS

Monotonic and cyclic tests were conducted on surrogate rods made of a Zry-4-clad tube and alumina pellets, including ones with and without epoxy bonds. The conclusions drawn based on the test results and initial data analysis are as follows:

- The surrogate rod with an epoxy bond appeared to be much stronger than the rod without the bond for both monotonic and cyclic loading cases. The epoxy-bond rod exhibited a brittle failure, while no appreciable failure could be seen for the rod without an epoxy bond even though the curvature of the rod reached the equivalent deformation level.

- The surrogate rods with an epoxy bond fractured under cyclic bending for load amplitudes greater than 100 N, with a lifetime between 10^4 and 10^6 loading cycles. No failure was seen at the 100 N load level at loading cycles up to two million cycles. An S-N curve is clearly defined for the cyclic test of epoxy-bond rods.

- The use of 10 Hz frequency in the cyclic test apparently accelerated the fatigue aging, which shortened the lifetime of the surrogate rod under a defined load level. A more detailed analysis regarding the potential dynamic inertia effect on the experimental results is needed; this action item can provide further benchmarks and clarification to the fatigue data obtained at higher-frequency bend loading conditions.

- No defined S-N trend was obtained for the rods without an epoxy bond, which could be the result of the uncertainties in the specimen machining condition, gap configuration at pellet–pellet and pellet–clad interfaces, and the use of various testing conditions.

8. REFERENCES

1. J.-A. J. Wang et al., *High Burn-Up Spent Fuel Vibration Integrity Study Progress Letter Report (Out-of-Cell Fatigue Testing Development – Task 2.1)*, ORNL/ TM-2010/288, Oak Ridge National Laboratory, Oak Ridge, TN, 2011.
2. J.-A. J. Wang et al., *Progress Letter Report on U-Frame Test Setup and Bending Fatigue Test for Vibration Integrity Study (Out-of-Cell Fatigue Testing Development – Task 2.2)*, ORNL/TM-2011/531, Oak Ridge National Laboratory, Oak Ridge, TN, 2012
3. J.-A. J. Wang et al., *Progress Letter Report on U-Frame Test Setup and Bending Fatigue Test for Vibration Integrity Study (Out-of-Cell Fatigue Testing Development – Task 2.3)*, ORNL/TM-2012/417, Oak Ridge National Laboratory, Oak Ridge, TN, 2012.
4. J.-A. J. Wang et al., *Progress Letter Report on Bending Fatigue Test System Development for Spent Nuclear Fuel Vibration Integrity Study (Out-of-Cell Fatigue Testing Development – Task 2.4)*, ORNL/TM- 2013/225, Oak Ridge National Laboratory, Oak Ridge, TN, 2013.
5. H. Wang et al., "Development of U-frame bending system for studying the vibration integrity of spent nuclear fuel," *Journal of Nuclear Materials* 440, 201–213 (2013).